Supplementary Information (SI) Appendix

For

Molecular Mechanism of Zn^{2+} Inhibition of a Voltage-Gated Proton Channel

by

Feng Qiu, Adam Chamberlin, Briana M. Watkins, Alina Ionescu, Marta Elena Perez, Rene Barro-Soria, Carlos Gonzalez

Sergei Y. Noskov, and H. Peter Larsson

Supplementary Figures

Figure S1. Zn^{2+} effect and kinetic model of wt Hv1. A) Normalized tail currents (I_{tail}/I_{max}) versus voltage curves for wt Hv1 channels in the presence of increasing extracellular Zn^{2+} concentrations (n = 4). B) Proposed model for Hv1 channel gating (only one subunit is shown for simplicity). In response to a depolarizing voltage pulse, Hv1 undergoes two different types of conformational changes (1): 1) first a slow conformational change of S4 from the resting closed state to the activated closed state, which decreases the fluorescence; 2) a second conformational change opens the Hv1 channel and increases the fluorescence to an intermediate fluorescence. C) Fluorescence simulations of the full model (solid red line) and for the model in the presence of an inhibitor that prevents the second (opening) step (dashed lines) in response to a voltage step to +80 mV from a holding voltage of -60 mV (solid black line).

Figure S2. Currents are inhibited at lower Zn^{2+} concentrations than the fluorescence. A-E) Current and fluorescence at the indicated voltage in response to increasing Zn^{2+} concentrations (Data from Figure 1B and F) fitted with a dose response curve. F) Fitted IC50 values (from A-E). The data is fitted with the IC50(V) = IC50(0mV) * exp($z\delta$*V/kT), with $z = 2e_0$. $\delta = 0.28 \pm 0.02$ for currents and $\delta = 0.18 \pm 0.02$ for fluorescence.

Figure S3. Different fluorophores report similar effects of Zn^{2+}. A) Structures of Alexa488-maleimide and TetramethylRhodamine-methane-thiosulfonate (TMR-MTS) attached to a cysteine (cys). B) Fluorescence changes (ΔF) from TMR-MTS-labeled S242C HV1 channels in response to a +80-mV voltage pulse in the presence of increasing extracellular Zn^{2+} concentrations. Note that low concentrations of Zn^{2+} decrease the fluorescence during the +80 mV pulse without altering the tail fluorescence, thereby decreasing the fluorescence hook. Higher Zn^{2+} concentrations decrease the total amplitude of the fluorescence change and inhibit the fluorescence hook completely.

Figure S4. Zn^{2+} inhibits outward S4 movement. A-B) Currents from N264C Ci-Hv1 channels in excised inside-out patches in response to the voltage and pH protocols shown above during repeated applications of 1 mM intracellular MTSET at +80 mV A) in the presence of 100 μM extracellular Zn^{2+} in the pipette solution and B) in the absence of extracellular Zn^{2+}. We first perfuse the channel with intracellular pH 5.5 to be able to measure the currents even in the presence of 100 μM Zn^{2+}. We hold the channels at -60 mV, then pulse the channels to +100 mV (at t = 10 ms; red dashed circle; magnified view to the right) to open the channels to measure the currents, and then hyperpolarize the channel to -60 mV (at t = 60 ms). Note that, at pH 5.5, some channels are open at -60 mV (star in B), due to that intracellular pH 5.5 shifts the voltage dependence of Hv1 channels by around -70 mV compared to at pH 7. 100 μM Zn^{2+} blocks the current at -60 mV (star in A), but still allows channels to open at +100 mV. We then switch to

intracellular pH 7.0 (t = 1000 ms) to be able to determine the effect of extracellular Zn^{2+} in physiological conditions. At 6000 ms, we depolarize to +80 mV and then apply 1 mM MTSET for 1 second (bar at top of protocol). Note that at +80 mV, Hv1 channels do not open significantly in the presence of 100 μM Zn^{2+} (** in B), but open in the absence of extracellular Zn^{2+} (** in A). We then wash out MTSET with pH 7.0 solutions. We next switch to pH 5.5 at 8000 ms to test the speed of the perfusion. Only patches where perfusion was faster than 200 ms was used in the analysis. Current spikes in B are perfusion artifacts, due to that in the transition from the pH 7 solution tube to pH 7 + MTSET tube the pH 5.5 perfusion tube is transiently in front of the patch. (A-B, right) Magnification of the currents during the +100 mV pulses in the recording on the left. MTSET modification of N264C abolishes the current (arrow in A; ref). C) Normalized currents measured at the arrow in A and B plotted against exposure to MTSET (in units of mM s). Intracellular MTSET quickly reduces the current at +80 mV in the presence of extracellular Zn^{2+} (■), compared to in the absence of Zn^{2+} (○). D) Cartoons showing (left) the proposed outward movement of S4 in the absence of Zn^{2+} (0 Zn^{2+}) in response to a depolarization, and (right) the inhibition of outward S4 movement in the presence of 100 μM Zn^{2+} (100 Zn^{2+}).

Figure S5. Zn^{2+} effect on E167A Hv1. A) Normalized tail currents (I_{tail}/I_{max}) versus voltage curves for E167A Hv1 channels in the presence of increasing extracellular Zn^{2+} concentrations (n = 4).

Figure S6. D233N selectively removes the Zn^{2+} inhibition of the S4 movement. A-B) Currents and fluorescence changes (ΔF/F) from Alexa488maleimide-labeled D233N/S242C in response to a +100-mV voltage pulse in the presence and absence of 100 μM Zn^{2+}. C) Normalized fluorescence changes ($\Delta F_{tail}/\Delta F_{max}$) versus voltage curves from D233N/S242C in the absence and presence of 100 μM Zn^{2+} (n = 4). D) BCECF fluorescence from oocytes expressing D233N channels that have been incubated with BCECF in response to a voltage step to +100 mV in the presence and absence of 100 μM Zn^{2+}.

Figure S7. Zn^{2+} affects fluorescence in H188A/S242C channels. A) Normalized tail currents (I_{tail}/I_{max}) versus voltage curves in the presence of increasing extracellular Zn^{2+} concentrations for H188A/S242C channels (n = 3). The curves are normalized to the maximum tail current (I_{max}) in ND96 control solution. B) Normalized fluorescence changes ($\Delta F_{tail}/\Delta F_{max}$) versus voltage curves in the presence of increasing extracellular Zn^{2+} concentrations (n=3). C) Fluorescence changes (ΔF) in response to a +80-mV voltage pulse in the presence of increasing extracellular Zn^{2+} concentrations. D) 1 μM Zn^{2+} increases the absolute change in the fluorescence signal during the +80-mV pulse, but does not alter the tail fluorescence. E) 10 μM Zn^{2+} further increases the absolute change in the fluorescence signal during the +80-mV pulse, but decreases the amplitude of the tail fluorescence. F) 100 μM Zn^{2+} decreases further the amplitude of the tail fluorescence.

Figure S8. D171A does not affect the Zn^{2+} inhibition of Hv1. A) Currents (top) and fluorescence (bottom) in response to a +80-mV voltage pulse in the presence of increasing extracellular Zn^{2+} concentrations on Alexa488maleimide-labeled Hv1 D171A/S242C channels. B) Normalized fluorescence changes ($\Delta F_{tail}/\Delta F_{max}$) versus voltage curves in the presence of increasing extracellular Zn^{2+} concentrations (n=4).

Figure S9. Fast perfusion in two-electrode voltage clamp experiments. Currents in response to a voltage step to +80 mV in pH = 7.4 (100 mM HEPES) in a two-electrode voltage clamp experiments on an oocyte expressing Ci-Hv1 channels. During the voltage pulse, pH was changed to pH 6.0 (100 mM MES) and back to pH 7.4 (100 mM HEPES), using a fast perfusion system as in Figure 5D. The response of the current in response to the pH changes was fitted with an exponential with $\tau = 0.63 \pm 0.17$ s (n = 3). Note that solution exchanges in Figures 2B and 3E were done with a slower perfusion system in the voltage clamp fluorometry set-up with a water immersion objective.

Figure S10. E167A and H188A have similar effects on Zn^{2+} inhibition of monomeric and dimeric Hv1 channels. A) Normalized fluorescence changes ($\Delta F_{tail}/\Delta F_{max}$) versus voltage curves for E167A/S242C/ΔNΔC channels in the presence of increasing extracellular Zn^{2+} concentrations (n = 4) . B) BCECF fluorescence from oocytes expressing E167A/S242C/ΔNΔC channels that have been incubated with BCECF in response to a voltage step to +100 mV in the presence and absence of 100 μM Zn^{2+}. C-D) Normalized tail currents (I_{tail}/I_{max}) versus voltage curves for C) H188A ΔNΔC and D) H188A/S242C/ΔNΔC channels in the presence of increasing extracellular Zn^{2+} concentrations (n=4).

Figure S11. Molecular model of Zn^{2+} binding to hHv1 and cHv1. **Top Panel: Model of Ci-Hv1 in its closed stated** embedded within a lipid bilayer with two Zn^{2+} ions bound (red and blue spheres). K+ and Cl- counterions are shown as magenta and green spheres, respectively. Phospholipids are shown as grey sticks with positions of the head-groups mapped by yellow spheres. **Bottom panel: Potential of Mean Force (PMF) for Zn^{2+} binding to the closed-activated state of mHv1 (purple line) and Ci-Hv1 channels (green line)** with Drude polarizable force-field. The residues and water molecules directly coordinating in the proposed binding sites are shown in sticks. The residues forming Zn^{2+} binding site in mHv1 crystal structure **(2)** are shown as red spheres. The bound Zn^{2+} ions are shown as blue spheres.

Figure S12. Proposed model for Zn^{2+} binding to the different states of the Hv1 channel (only one subunit is shown for simplicity). In response to a depolarizing voltage pulse in the absence of Zn^{2+} (middle row of states), Hv1 undergoes two different types of conformational changes (1): 1) first a slow conformational change of S4 from the resting closed state to the activated closed state, which decreases the fluorescence; 2) a second conformational change opens the

Hv1 channel and increases the fluorescence to an intermediate fluorescence. In the presence of low concentrations of Zn^{2+} (bottom row), Zn^{2+} binds to site1, which prevents channel opening. At high concentrations of Zn^{2+} (2 top rows), Zn^{2+} binds to site2, which prevents outward S4 movement. In addition, Zn^{2+} can bind to both Site 1 and Site 2 (top row). Rate constants are given in Supplementary Table S1. $Zn'_{ON1} = Zn_{ON1}$ and $Zn'_{Off1} = Zn_{Off1}/B$, while $\alpha' = \alpha$ and $\beta' = \beta * B$ to maintain detailed balance.

Figure S13. Kinetic model reproduce the effect of Zn^{2+} on wt and mutant channels. A, C, and E) Simulations of the currents (top) and fluorescence (bottom) in response to a +80-mV voltage pulse in the presence of increasing extracellular Zn^{2+} concentrations for A) wt Hv1, C) Hv1 E167A, and E) Hv1 D233N model channels, using the kinetic models shown in Supplementary Figure S12. B, D, and F) Tail currents (I) versus voltage curves and fluorescence (F) versus voltage curves for B) wt Hv1, D) Hv1 E167A, and F) Hv1 D233N model channels in the presence of increasing extracellular Zn^{2+} concentrations from simulations in A, C, and E, respectively. Note the different current scale in E compared to A and C, showing a lower open probability for D233N channels.

Figure S14. E241H does not increase the Zn^{2+} affinity. A) Normalized tail currents (I_{tail}/I_{max}) versus voltage curves for E241H Ci-Hv1 channels in the presence of increasing extracellular Zn^{2+} concentrations (n = 4). The curves are normalized to the tail current (I_{max}) at +100mV in ND96 control solution. B) Currents at +40 mV in response to increasing Zn^{2+} concentrations (Data from A) fitted with a dose response curve.

References

1. Qiu F, Rebolledo S, Gonzalez C, & Larsson HP (2013) Subunit interactions during cooperative opening of voltage-gated proton channels. *Neuron* 77(2):288-298.
2. Takeshita K*, et al.* (2014) X-ray crystal structure of voltage-gated proton channel. *Nature structural & molecular biology* 21(4):352-357.

Transition	wt	E167A	D233N
α	0.01 exp(1.6e_0V/kT)	0.01 exp(1.6 e_0V/kT)	0.01 exp(1.6 e_0V/kT)
β	2.9 exp(-0.8 e_0V/kT V)	2.9 exp(-0.8 e_0V/kT)	2.9 exp(-0.8 e_0V/kT)
γ	1 exp(1 e_0V/kT)	1 exp(1 e_0V/kT)	0.01 exp(1 e_0V/kT)
δ	30 exp(-0.45 e_0V/kT)	1.5 exp(-0.45 e_0V/kT)	10 exp(-0.45 e_0V/kT)
Zn_{ON1}	0.1	0.05	0.05
Zn_{OFF1}	0.1	0.5	5
Zn_{ON2}	0.05	0.05	0.05
Zn_{OFF2}	0.25	>100	>100
B	0.2	0.1	1

Supplementary Table S1. Model rates. Rates in the model in Supplementary Figure S12, used for the simulations in Supplementary Figure S13. V is the voltage. Rate constants in [s^{-1}], except for Zn_{ON1} and Zn_{ON2} [μM^{-1} s^{-1}] and B, which is only a constant factor. The rate constants α, β, γ, and δ for wt Hv1 channels were determined in a previous study (1).

Supplementary Figure S1.

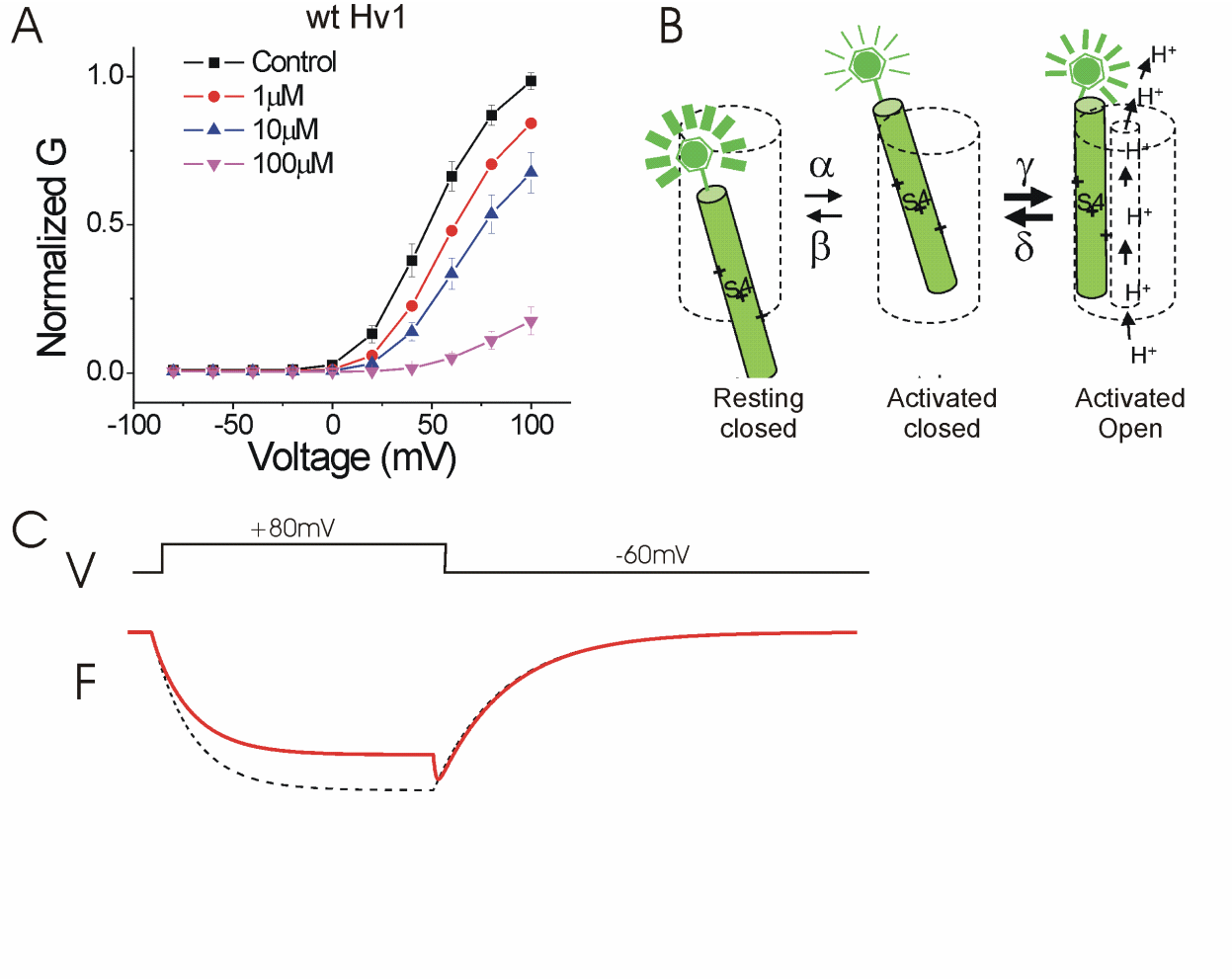

Supplementary Figure S2.

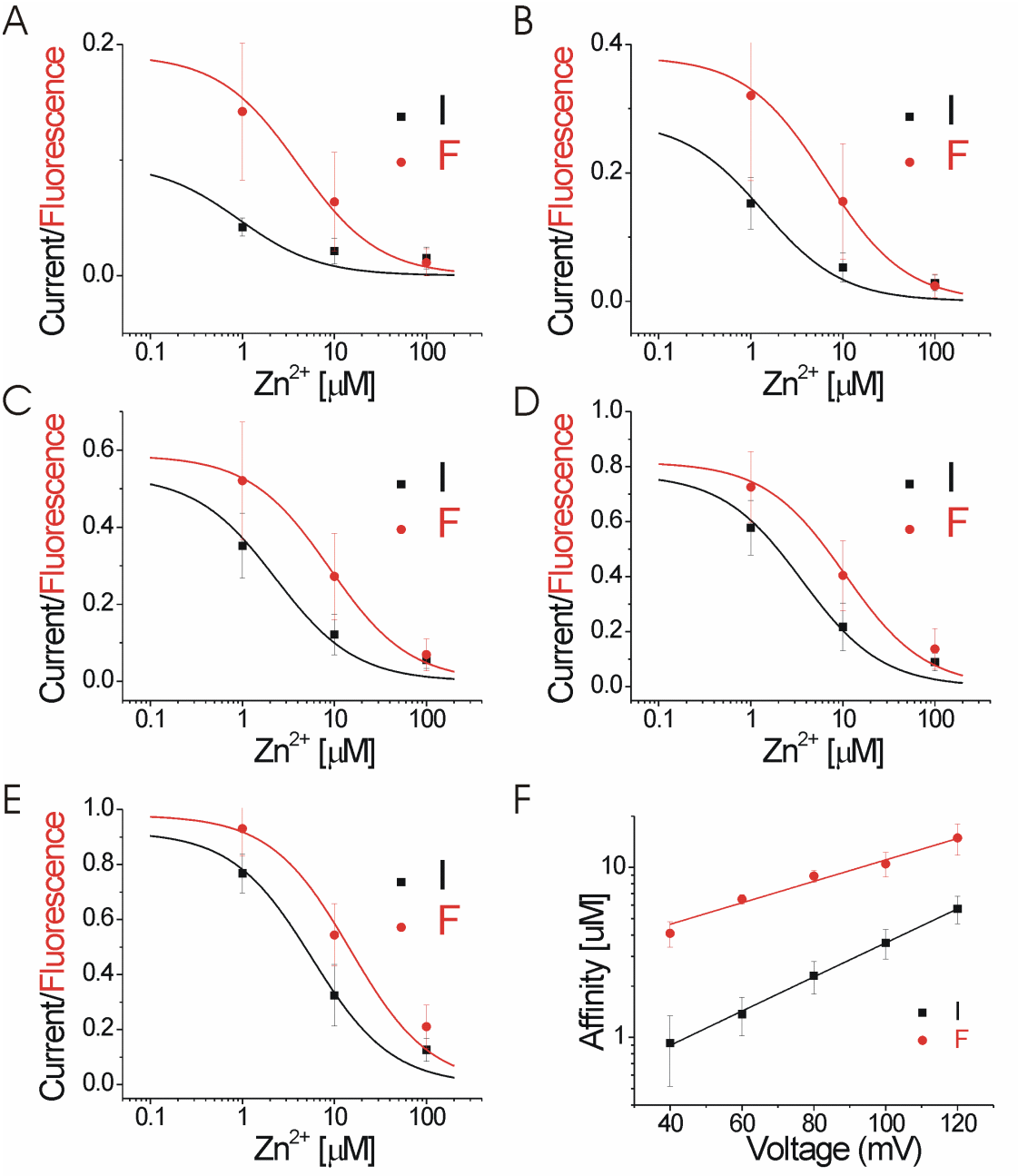

Supplementary Figure S3.

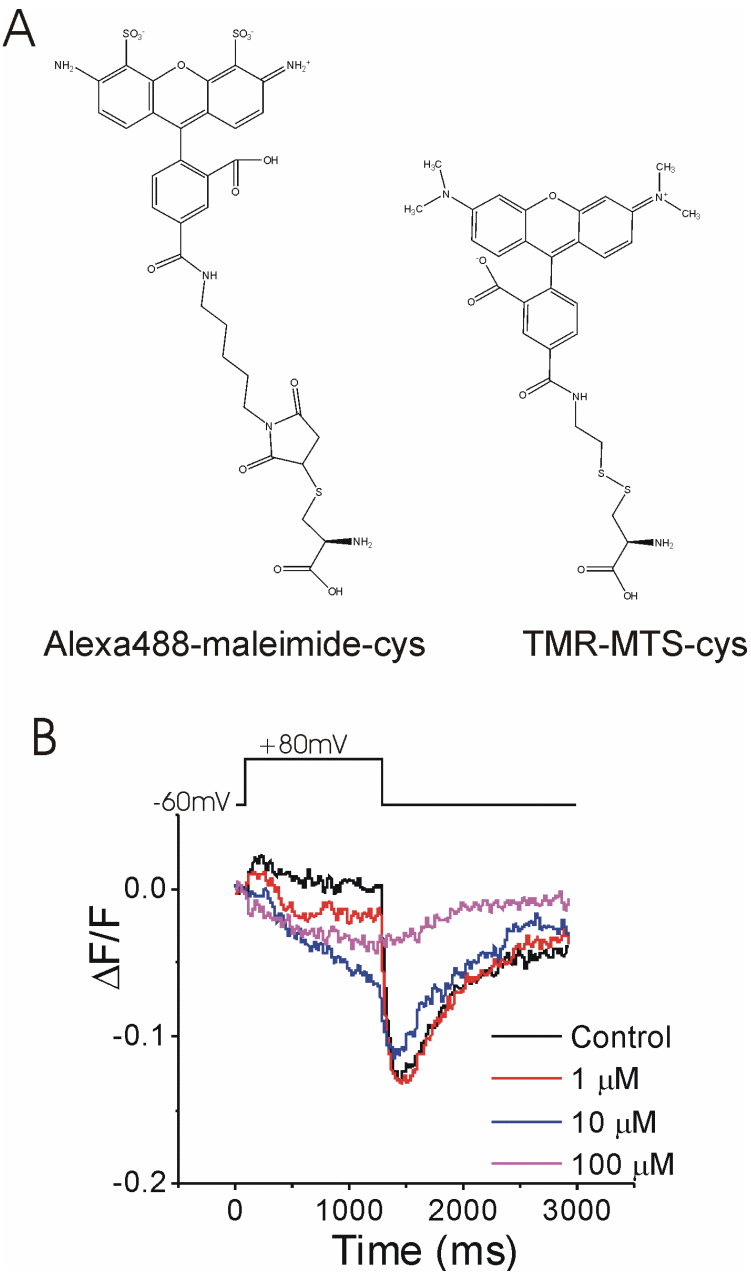

Supplementary Figure S4.

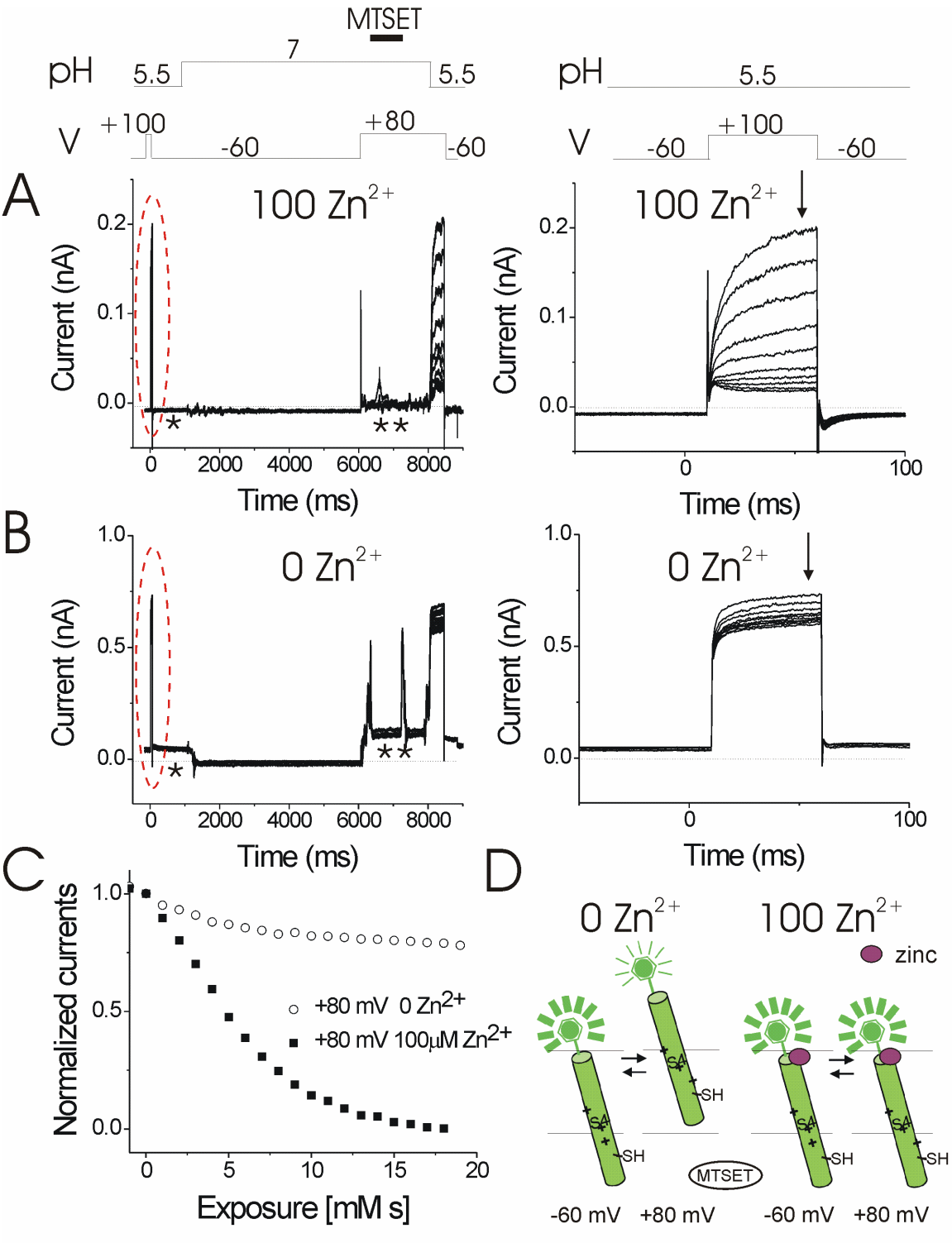

Supplementary Figure S5.

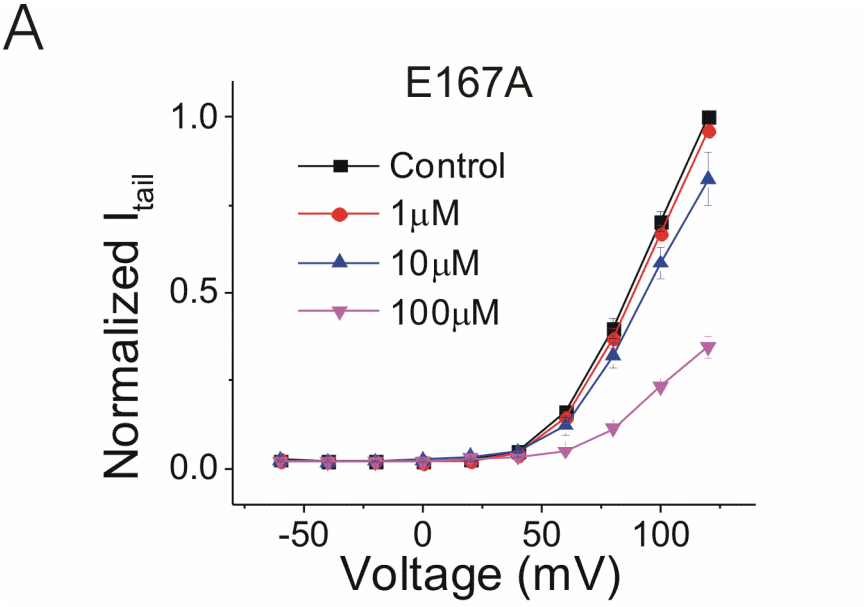

Supplementary Figure S6.

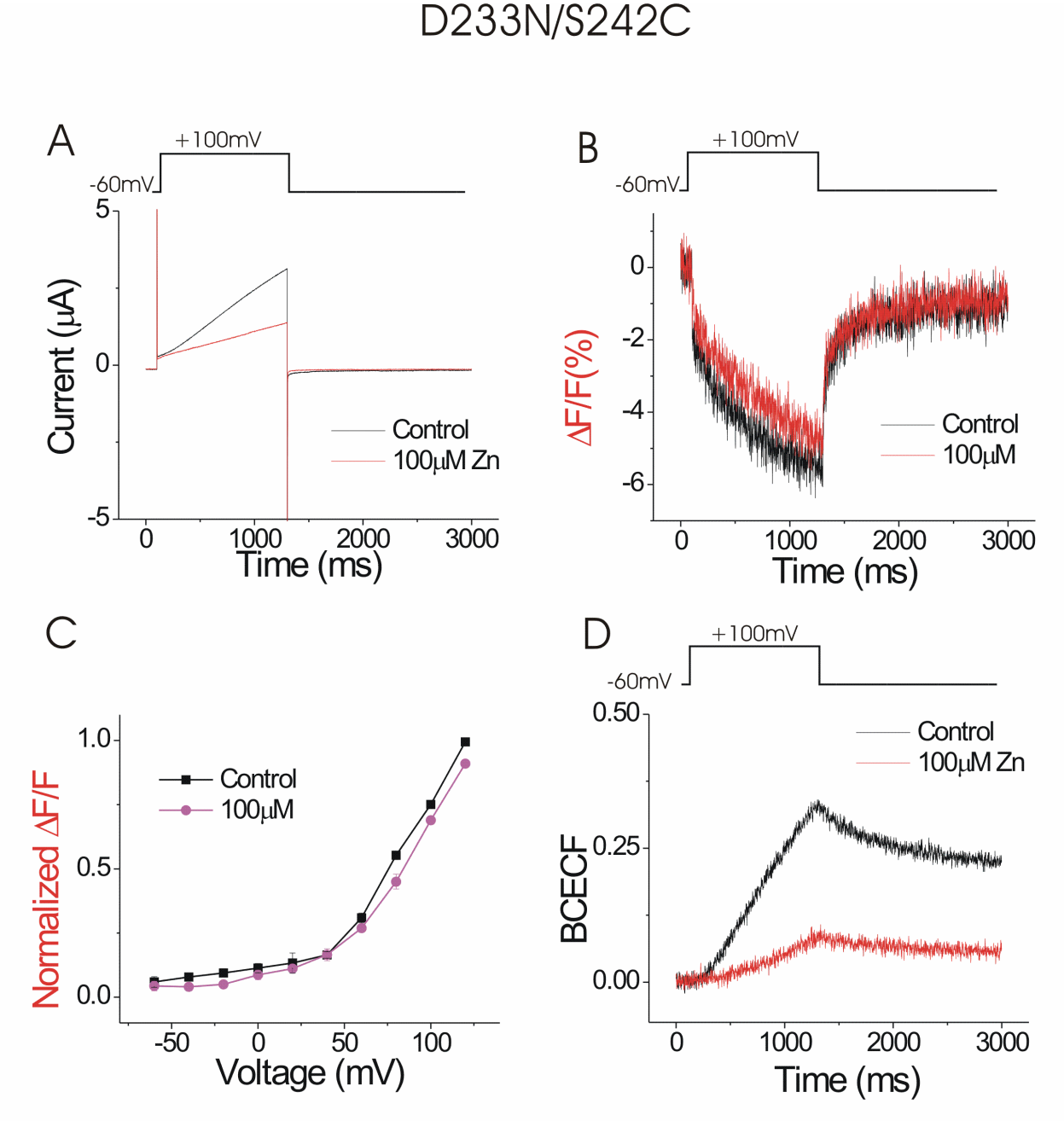

Supplementary Figure S7.

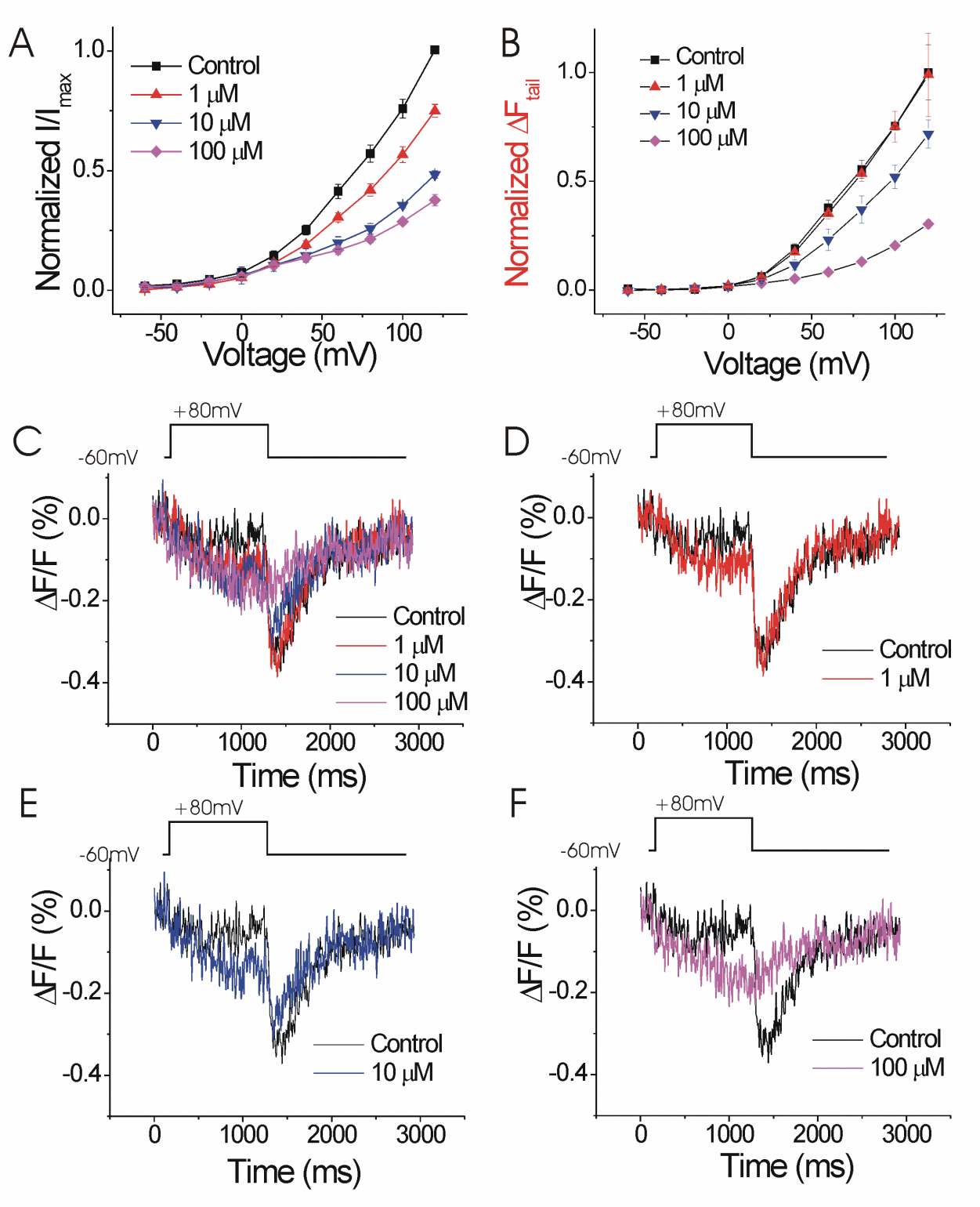

Supplementary Figure S8.

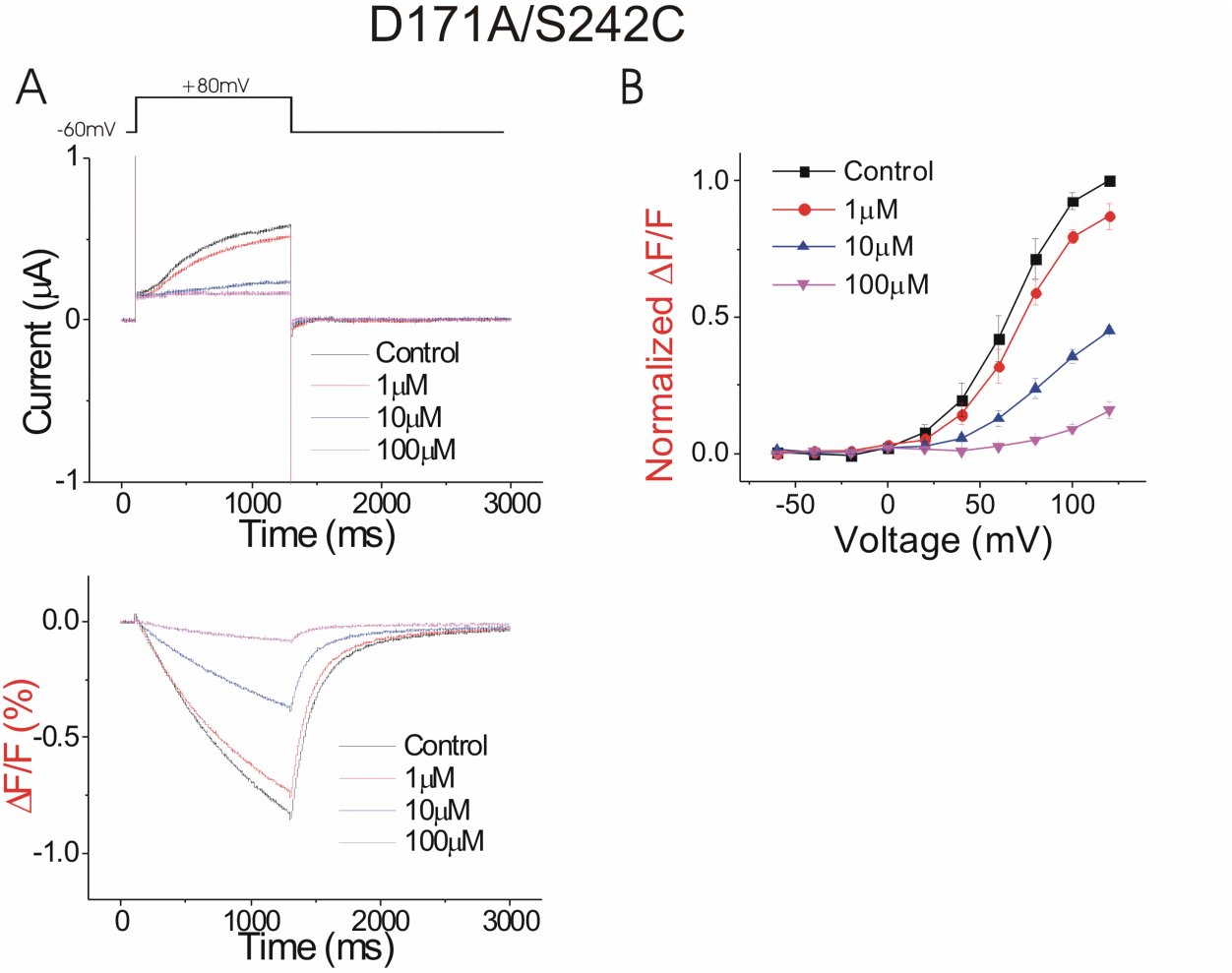

Supplementary Figure S9.

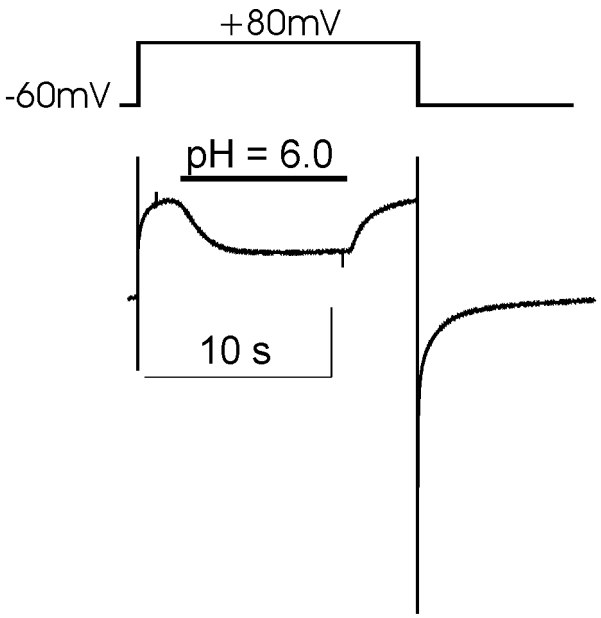

Supplementary Figure S10.

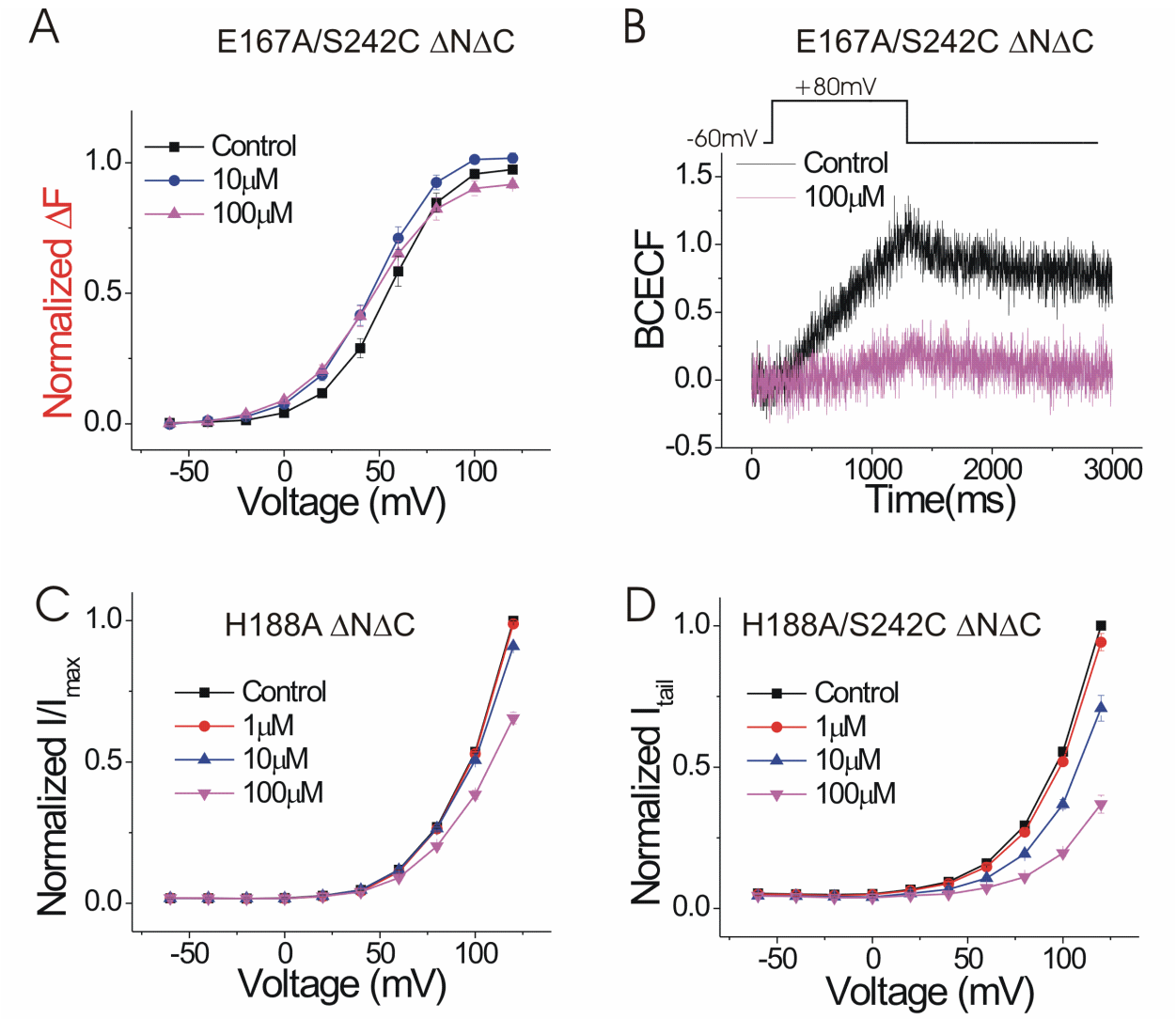

Supplementary Figure S11.

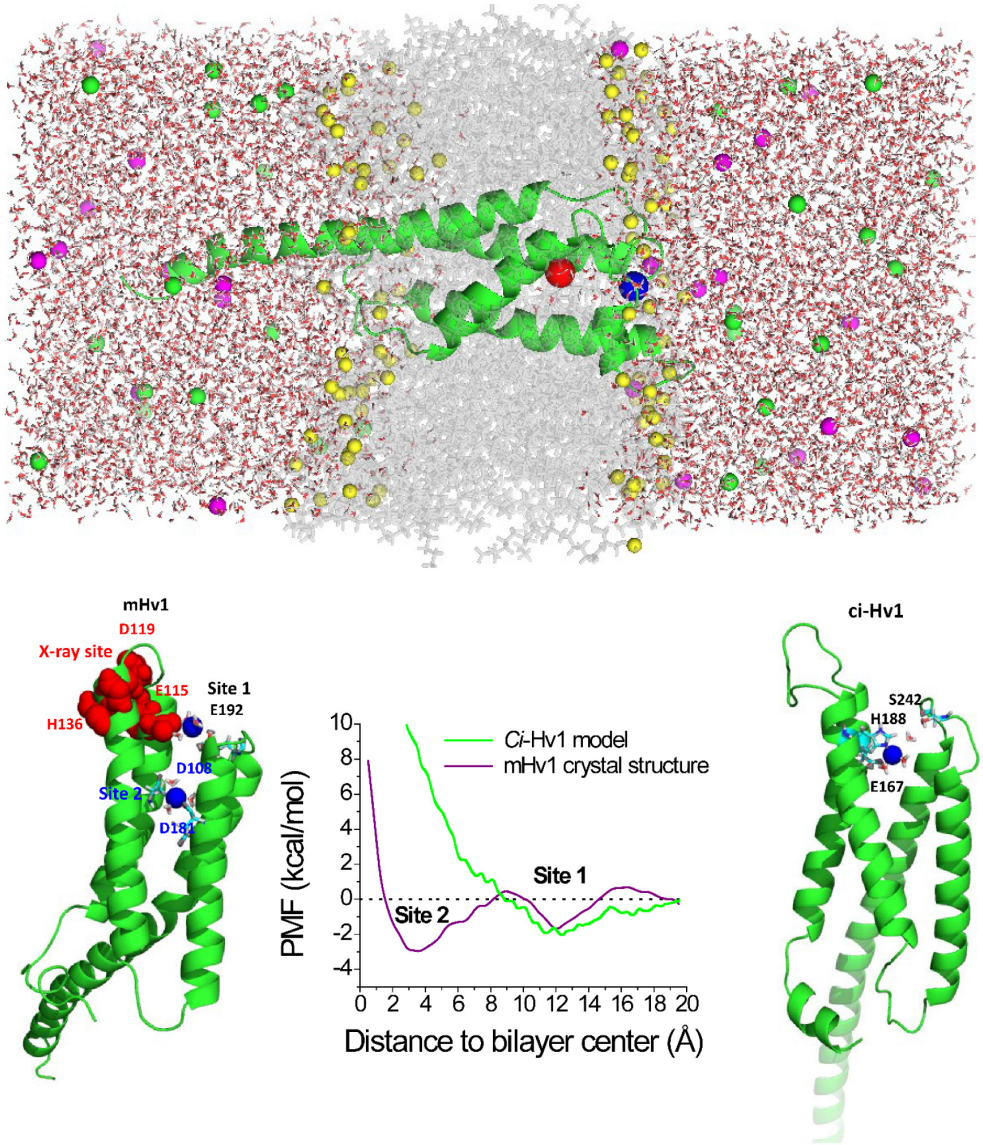

Supplementary Figure S12.

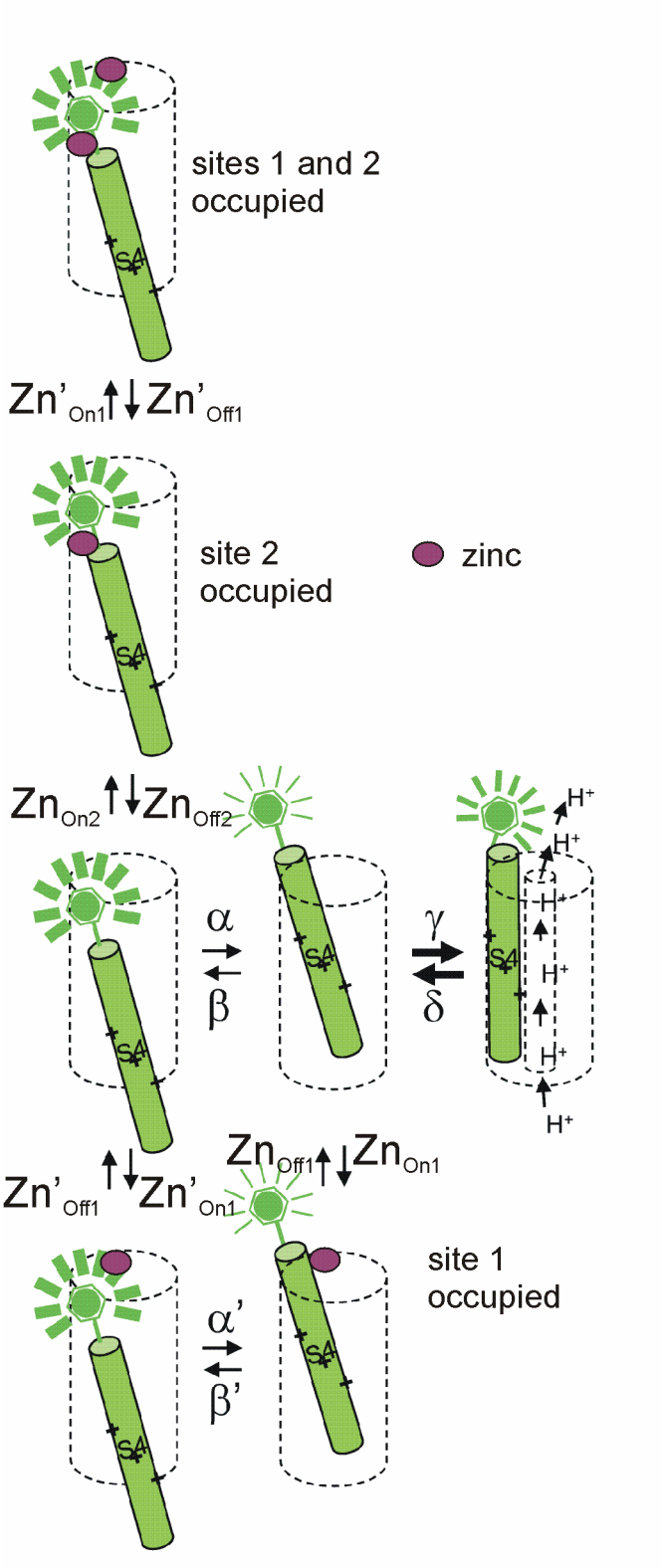

Supplementary Figure S13.

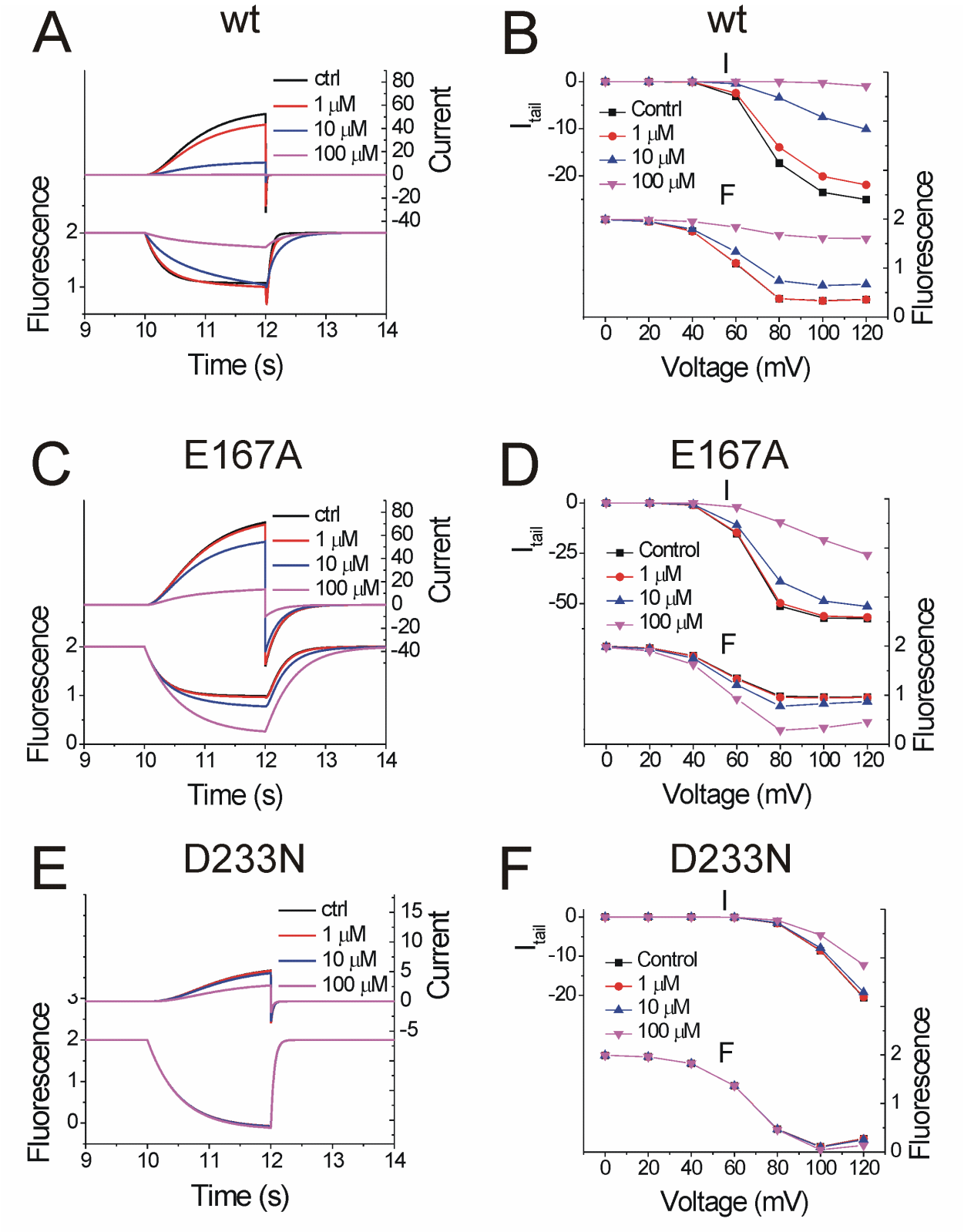

Supplementary Figure S14.